

Constraining coronal magnetic field models using coronal polarimetry

K. Dalmasse, D. W. Nychka, S. E. Gibson, N. Flyer & Y. Fan

NCAR, P.O. Box 3000, Boulder, CO 80307-3000, USA; dalmasse@ucar.edu

1. Abstract

- Knowing the 3D coronal magnetic field prior to the trigger of a coronal mass ejection (CME) is one of the key features for predicting their geomagnetic effect. Since the magnetic field is essentially measured at the photosphere, one must rely on models to obtain the 3D magnetic field in the corona. Various coronal observables can then be used to constrain the parameters, and hence the magnetic field, of these models.
- In this regard, one type of observable that is receiving an increasing attention is coronal polarization of infrared lines such as the Fe XIII 10747 Å and 10798 Å lines observed by the Coronal Multichannel Polarimeter (CoMP), which are sensitive to the coronal magnetic field. By combining forward modeling with a novel optimization method applied to a synthetic test bed of a coronal magnetic flux rope, we show that the polarimetric signal of coronal infrared lines contains enough information to constrain the parameters, and hence the magnetic structure, of coronal magnetic field models.

2. Coronal polarimetry of Fe XIII

- The infrared Fe XIII-I (10747 Å) and XIII-II (10798 Å) lines are sensitive to the Zeeman effect (frequency-modulated polarization) and the Hanle effect (depolarization of scattered light, as illustrated in Fig. 1; Casini & Judge 1999), such that the linear (respectively, circular) polarization is dominated by the Hanle (respectively, Zeeman; e.g., Judge *et al.* 2006) effect.

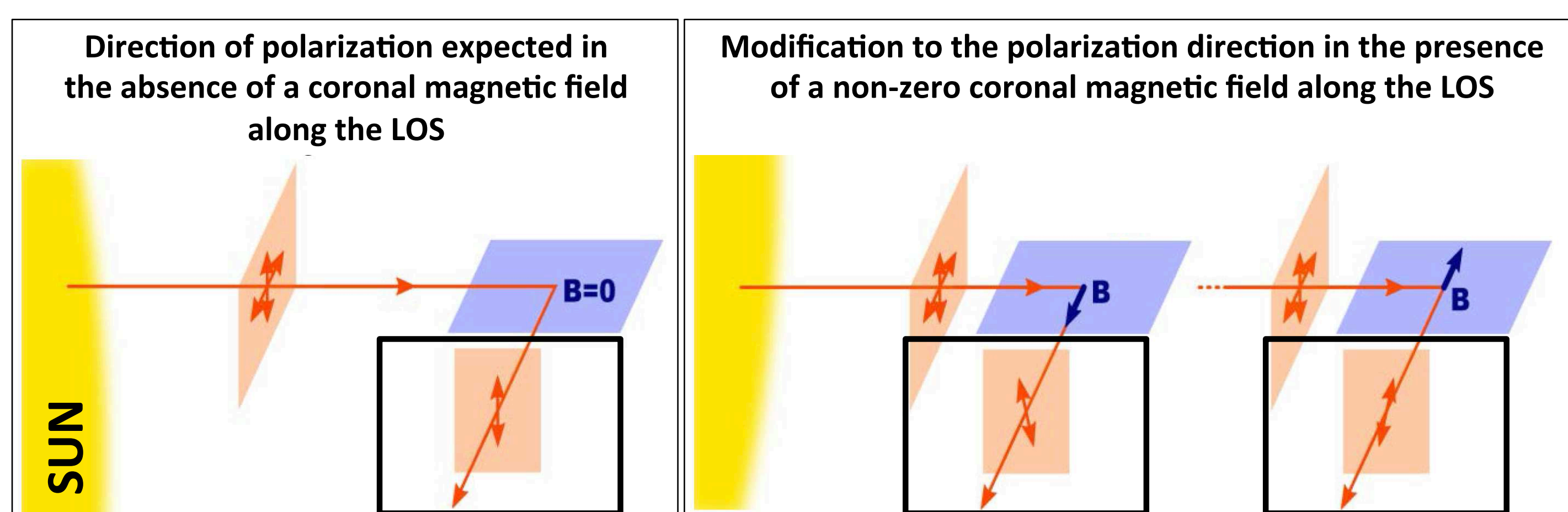


Figure 1: Illustration of the Hanle effect on the direction of coronal linear polarization observed at the solar limb (adapted from Trujillo Bueno *et al.* 2005).

- The Coronal Multichannel Polarimeter (CoMP; Tomczyk *et al.* 2008) provides routine measurements of the linear polarization (Stokes Q and U) and line intensity (Stokes I) for these lines.
- Inverting such polarimetric measurements into magnetic field data is a difficult task because (a) the linear polarization for these lines is sensitive to the magnetic field direction but not its strength (saturated Hanle effect; Casini & Judge 1999); and (b) the corona is optically thin at these wavelengths.
- Fig. 2 nonetheless shows that such linear polarization signal contains enough information to distinguish (c) different magnetic field topologies (Rachmeler *et al.* 2013, 2014), and (d) different magnetic fields of the same topology but with different parameters (e.g., orientation).

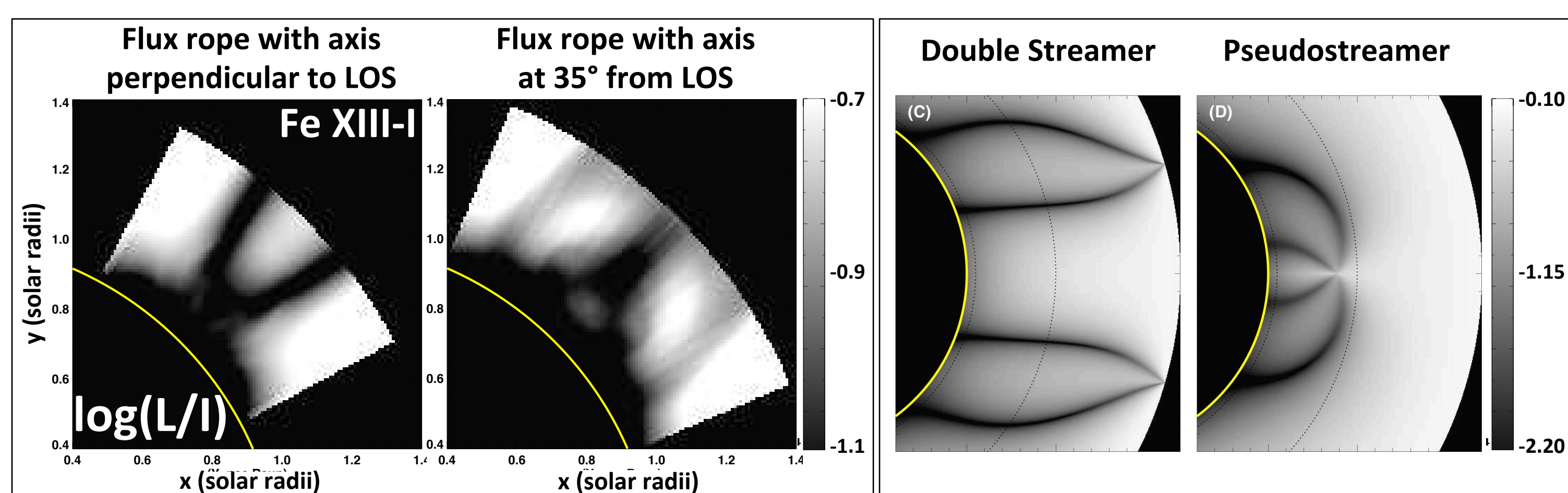
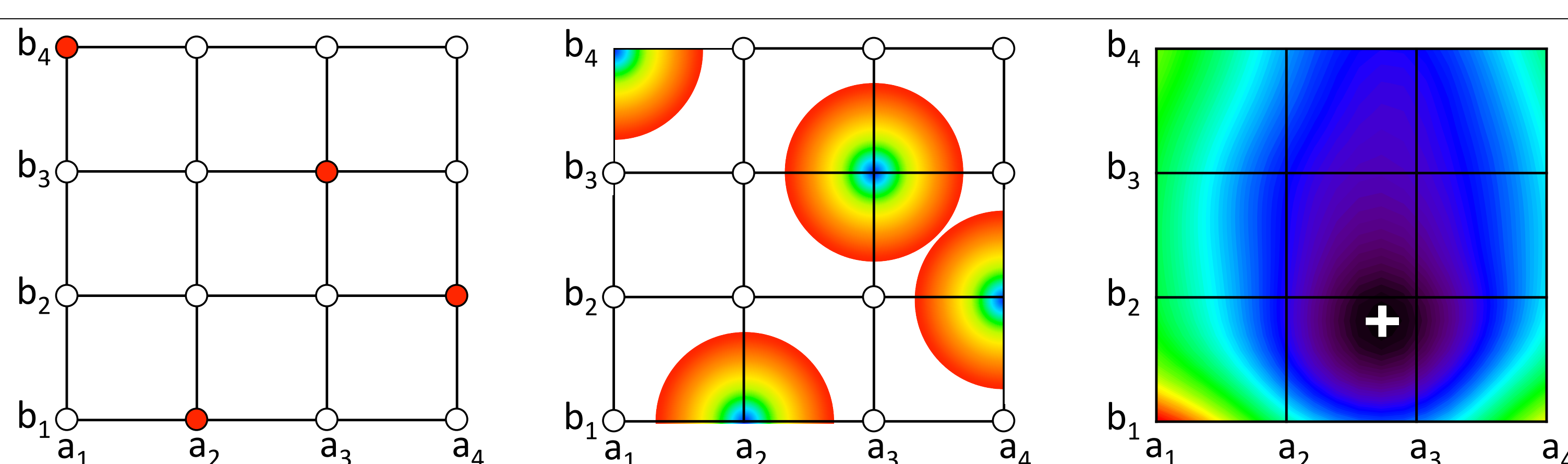


Figure 2: Examples of 2D, line-of-sight (LOS) integrated maps showing the effect of magnetic topology and orientation of the magnetic field (with regard to the observer) on the percentage of linear polarization predicted for the Fe XIII-I infrared line (10747 Å). These polarization maps were generated using the FORWARD package of SolarSoft IDL (Gibson *et al.* 2016). Notice the polarization extinction signatures (van Vleck effect; van Vleck 1925) that allow to distinguish between different magnetic topologies and magnetic field orientations. For the twisted magnetic flux rope case, the magnetic field is displayed in Fig. 3(a). The Double Streamer and Pseudostreamer cases are from Rachmeler *et al.* (2014).

3. Model-data fitting using coronal polarimetry of Fe XIII

- To perform model-data fitting using the coronal polarimetry of Fe XIII, we combine:
 - The Coronal Line Emission (CLE) fortran polarimetry code developed by Judge & Casini (2001) that performs forward modeling of the Stokes (I, Q, U, V) line profiles – associated with a user-specified coronal model – for visible and infrared forbidden lines (Casini & Judge, 1999). CLE is integrated to the FORWARD package of SolarSoft IDL (Gibson *et al.* 2016)
 - An optimization method, ROAM (Radial-basis-function Optimization Approximation Method; see Fig. 3), that we recently developed for general, fast and efficient model-data fitting (Dalmasse *et al.*, submitted)



- Sparse sampling of the parameter space (McKay *et al.* 1979) to select n -couples of parameter values (red points) for which to compute the magnetic model and predicted polarization signal
- Compute the loss function (typically a χ^2) comparing the predicted polarization signal to the measured polarization
- Place a radial basis function (RBF; function that only depends on the distance to its center; e.g., Duchon 1976; Nychka *et al.* 2015) at each of point where the loss function has been computed
- RBF interpolation/reconstruction of the loss function
- Find an estimator of the best-fit parameters (white '+' sign) by minimizing the RBF-interpolated loss function using the DFPMIN IDL routine

Figure 3: Conceptual description of the ROAM for a 2D parameter space, (a,b), with a grid of 16 points. In the middle panel, the radial basis functions (RBFs) are plotted up to a radius, r , from their centers. Here, black/red shows the minimum/maximum loss function values.

4. Synthetic test bed with a 3D parameter space

- Fig. 4a presents the magnetic field of the synthetic test bed while Fig. 4b displays the three parameters used for testing the model-data fitting method using coronal polarimetry of the forbidden infrared Fe XIII line. The parameters relate to the position of the flux rope in the solar corona: (co-latitude ; longitude ; rotation angle) = $(\theta; \phi; \Omega)$.
- $(\theta_{GT}; \phi_{GT}; \Omega_{GT}) = (45^\circ; 90^\circ; 30^\circ)$ is chosen as the ground truth.
- All line-of-sight (LOS) integrated, synthetic images of the polarization signal employed with this test bed are generated using the CLE (cf. Section 3).

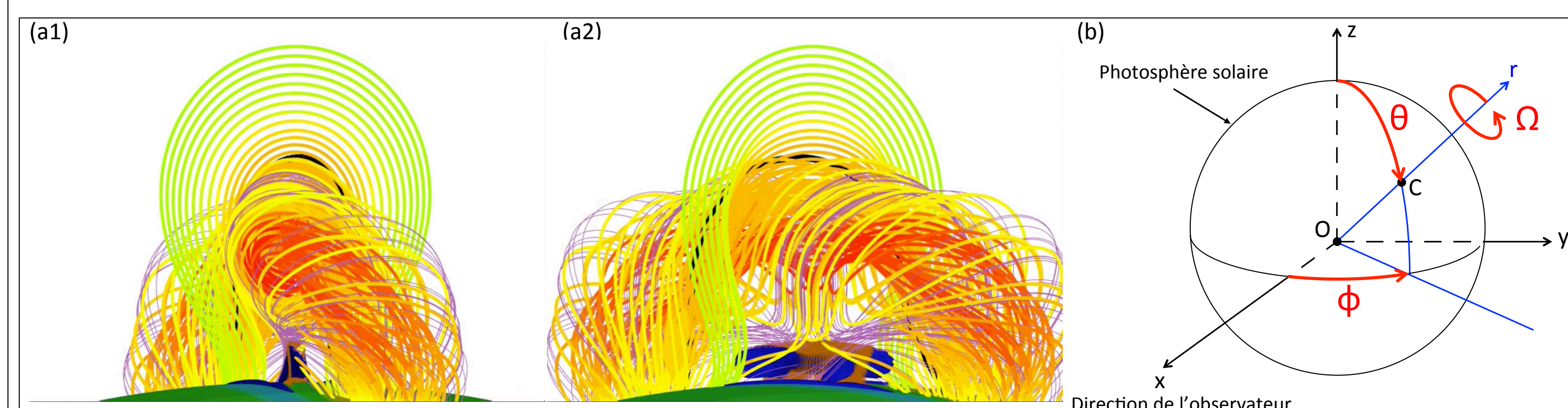


Figure 4: (a) Twisted magnetic flux rope considered for the test case as seen from different rotation angles, $\Omega = -5^\circ$ (a1) and $\Omega = 90^\circ$ (a2). (b) Schematic describing the three parameters considered for the tests performed to validate the model-data fitting method described Section 3. Point C corresponds to the photospheric center of the numerical box containing the magnetic field. Point O is the center of the Sun. The solid black sphere highlights the solar photosphere.

5. Results

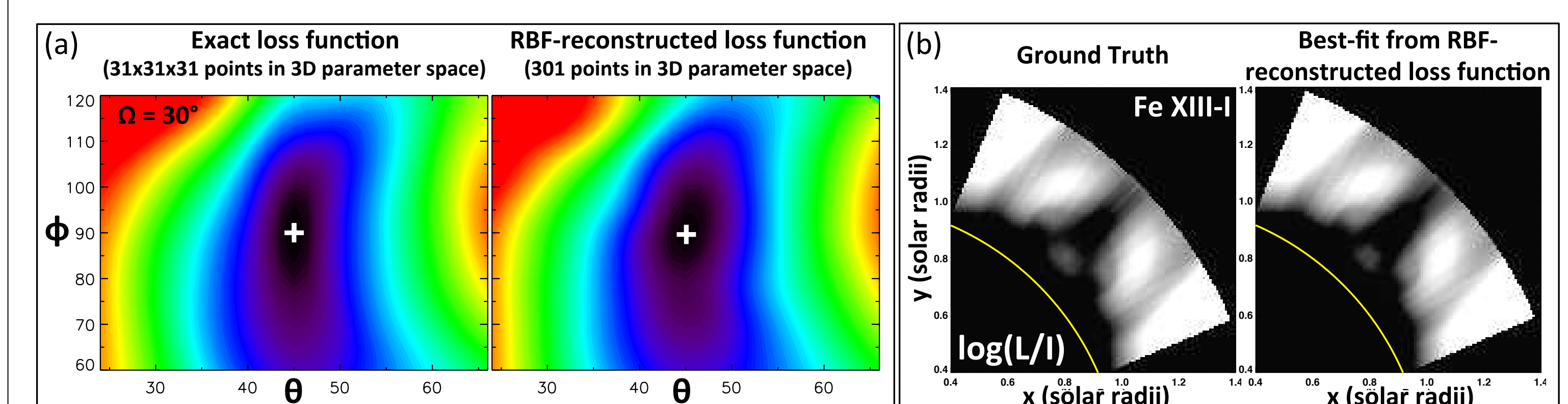


Figure 5: Examples of 2D cuts of the exact and RBF-interpolated, 3D loss function. The white '+' sign indicates the position of the minimum, and hence, best-fit parameters for which the percentage of linear polarization is shown in the two panels on the right.

- Fig. 5a shows that the RBF reconstruction gives a very good approximation of the exact loss function (rms error ≈ 0.05) while using 301 points (i.e., parameter triplets) distributed in the 3D parameter space instead of 31^3 .
- The best-fit parameters from the RBF reconstruction, $(45.0^\circ; 89.9^\circ; 30.3^\circ)$, provide an accurate estimation of the ground truth, $(\theta_{GT}; \phi_{GT}; \Omega_{GT}) = (45^\circ; 90^\circ; 30^\circ)$.
- The RBF reconstruction computed from 301 points in 3D parameter space is:
 - 100 times faster than a full grid search with 31^3 points;
 - 10^5 times faster than a full grid search with 301^3 points.
- Fig. 5b shows that the predicted polarization signal for the best-fit parameters obtained with the RBF reconstruction gives a good approximation of the ground truth; the error on the polarization signal is smaller than 0.005.

6. Conclusion & work-in-progress

- Our synthetic test bed show that (1) the coronal polarization data of the Fe XIII line observed at the solar limb can be used to constrain the morphology, orientation, and distribution of the associated 3D magnetic fields, and (2) our optimization method (ROAM) provides an interesting way for including more coronal data (provided that one can forward model them) into coronal magnetic field reconstructions.
- Our next step involves a synthetic test bed using the model-data fitting method presented Section 3 to fit a twisted flux tube with the magnetic field model (van Ballegoijen 2004) that we plan to use in future observational applications. Such test bed will allow us to assess the performance of our data-constrained reconstruction method of the solar coronal magnetic field in retrieving key quantities and properties for solar activity (e.g., electric currents, magnetic helicity, volumes of strong magnetic field gradients).

Acknowledgments

This work is part of the DOCFM (Data-Optimized Coronal Field Model; <http://www.hao.ucar.edu/DOCFM/>) project funded by the Air Force Office of Scientific Research (AFOSR). K.D. acknowledges funding from NCAR/CISL and NCAR/HAO, as well as support from the AFOSR under award FA9550-15-1-0030. NCAR is sponsored by the National Science Foundation.

References

- Casini, R. & Judge, P. G. 1999, *ApJ*, 522, 1, pp. 524-539
 Judge, P. G. & Casini, R. 2001, *ASP Conference Proceedings*, Vol. 236, pp. 503-510
 Dalmasse, K., Nychka, D. W., Gibson, S. E., *et al.*, submitted to *FrASS*
 Duchon, J. 1976, *Lecture Notes in Mathematics*, Vol. 571, pp. 85-100
 Fan, Y. 2012, *ApJ*, 758, 60
 Gibson, S. E., Kucera, T., White, S. M., *et al.* 2016, *FrASS*, 3, 8
 McKay, M. D., Beckman, R. J., and Conover, W. J. 1979, *Technometrics*, Vol. 21, No. 2, pp. 239-245
 Nychka, D. W., Bandyopadhyay, S., Hammerling, D., *et al.* 2015, *JCGS*, 24, 2, pp. 579-599
 Rachmeler, L. A., Gibson, S. E., Dove, J. B., *et al.* 2013, *Solar Physics*, 288, 2, pp. 617-636
 Rachmeler, L. A., Platten, S. J., Bethge, C., *et al.* 2014, *ApJL*, 787, 1, L3
 Tomczyk, S., Card, G. L., Darnell, T., *et al.* 2008, *Solar Physics*, 247, 2, pp. 411-428
 Trujillo Bueno, J., Landi Degl'Innocenti, E., Casini, R., *et al.* 2005, *ESASP*, 588, p. 203
 van Ballegoijen, A. A. 2004, *ApJ*, 612, 1, pp. 519-529
 van Vleck, J. H. 1925, *PNAS*, Vol. 11, 10, pp. 612-618